Vol 18 No 6, June 2009
1674-1056/2009/18(06)/2576-06
Chinese Physics B
© 2009 Chin. Phys. Soc.
and IOP Publishing Ltd

The electrical transport behavior of Zn-treated $Zn_{1-x}Mn_xO$ bulks*

Peng Xian-De(彭先德), Zhu Tao(朱 涛)†, Wang Fang-Wei(王芳卫), Huang Wan-Guo(黄万国), and Cheng Zhao-Hua(成昭华)

Beijing National Laboratory for Condensed Matter Physics, Institute of Physics, Chinese Academy of Sciences, Beijing 100190, China

(Received 6 January 2009; revised manuscript received 6 March 2009)

$Zn_{1-x}Mn_xO$ bulks have been prepared by the solid state reaction method. Zn vapor treatment has been carried out to adjust the carrier concentration. For the Zn treated $Zn_{1-x}Mn_xO$ bulks, analysis of the temperature dependence of resistance and the field dependence of magnetoresistance demonstrates that the bound magnetic polarons (BMPs) play an important role in the electrical transport behavior. The hopping of BMPs dominates the electrical conduction behavior when temperature is below 170 K. At low temperature, paramagnetic $Zn_{1-x}Mn_xO$ bulks show a large magnetoresistance effect, which indicates that the large magnetoresistance effect in transition-metal doped ZnO dilute magnetic semiconductors is independent of their magnetic states.

Keywords: Mn doped ZnO, x-ray, resistance, magnetoresistance
PACC: 7550P, 7530V, 6110M

1. Introduction

Unlike conventional semiconductors, diluted magnetic semiconductors (DMSs) take the advantage of not only the electron charge freedom but also the electron spin freedom.[1] The new generation electronic devices made of DMSs have the following advantages: increased data processing speed, decreased electric power consumption, increased integration densities, and so on. These new materials have been studied intensively in the past decades. Predicated by the theoretical prediction that transition-metal doped ZnO may exhibit room temperature ferromagnetism (FM),[2] ZnO based DMS become an attractive example.[2−5] Room temperature FM has been first reported in 3*d* metal doped ZnO thin films, and then in nanoparticles.[3−7] On the other hand, only the paramagnetic (PM) property has been reported in $Zn_{1-x}Mn_xO$ bulk samples.[8−12] Compared to the numerous studies on the thin films and nanoparticle of the Mn doped ZnO, the bulk samples have not been well studied, although it is believed that some intrinsic properties may be identified from the bulk samples. So we think that the study on the $Zn_{1-x}Mn_xO$ bulks should be intensified. Although there are some reports studying the $Zn_{1-x}Mn_xO$ bulks, the study of electrical transport behavior for the bulk samples is very deficient. This is because the as-prepared $Zn_{1-x}Mn_xO$ bulks are normally completely insulating. In this way, the measurement of the electrical transport cannot be carried out. In this work, we will overcome this shortage by Zn vapor treatment.

In our previous study,[13] the Zn treatment has been used to adjust the carrier concentration of Co doped ZnO bulks and the Zn treated $Zn_{1-x}Co_xO$ bulks show room temperature ferromagnetism. In this paper, we will use the same method to treat Mn doped ZnO bulks. After Zn vapor treatment, the $Zn_{1-x}Mn_xO$ bulks still show paramagnetic behavior, but it changes from insulator to semiconductor. Therefore, the electrical transport behavior can be systematically investigated.

2. Experiment

$Zn_{1-x}Mn_xO$ ($0 \leq x \leq 0.10$) bulks were synthesized by the solid state reaction method. High purity reactants (99.9%) of ZnO and MnO_2 (Alfa Aeasar, USA) with stoichiometric amount were thoroughly ground in a carnelian mortar and pressed into small pellets, and then annealed at 500 °C for 24 hours. The

*Project supported by the National Natural Science Foundation of China (Grant No 50871120).
†Corresponding author. E-mail: tzhu@aphy.iphy.ac.cn

annealed materials were reground, pressed to small pellets, and then sintered at 1200 °C for 24 hours to obtain the as-prepared samples. The as-prepared samples were subjected to the Zn treatment process, in which the samples were exposed in the Zn vapor and annealed at 500 °C for 8 hours.[13,14] X-ray diffraction (XRD) measurements were carried out using the D/Max-2400 (Cu Kα source). Magnetic properties were measured using a superconducting quantum interference device (SQUID, MPMS-7, Quantum Design TM). The resistances of the samples were measured with the standard four-pointed method on a physical properties measurement system (PPMS, Quantum Design TM).

3. Results and discussion

The XRD patterns of $Zn_{1-x}Mn_xO$ samples are shown in Fig.1. The log scale of diffraction intensity is used to show very small contributions of impurity phases. As shown in the figure, only the diffraction peaks of wurtzite structure can be observed when the Mn concentration is below 5%. The peaks show systematic shifts with the increase of doping concentration, which correspond to the changing of the lattice parameters. When the doping levels $x > 0.05$,

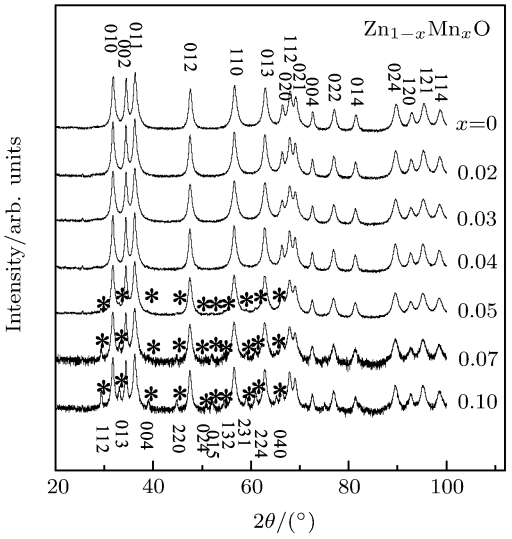


Fig.1. XRD patterns of $Zn_{1-x}Mn_xO$ (x = 0, 0.02, 0.03, 0.04, 0.05, 0.07 and 0.10) bulks. The mark * indicates the diffraction peaks of impurity phase $ZnMn_2O_4$.

the diffraction peaks of impurity phase $ZnMn_2O_4$ can be observed as marked by * in the patterns. As shown in the pattern, the peak intensity of these impurity phases increases with the increase of Mn content.

The Rietveld refinement process using the RIETICA code[15] was employed in the data refinement. In the fitting process, the space group $P63mc$ (wurtzite structure) was selected as the start model. The atomic sites were: Zn/Mn 2b(1/3, 2/3, 0) and O 2b(1/3, 2/3, z) respectively. The fractional occupancies of atomic position were fixed as the nominal stoichiometric values and were not refined. When $x > 0.05$, the impurity phase of $ZnMn_2O_4$ was considered in the refinement process. The refinement results are listed in Table 1. The small refinement factors (< 10%) indicate that the refinement results are reliable.

Figure 2 shows the Mn concentration dependence of the lattice parameters (a and c) and unit cell volume (V), respectively. As shown in Fig.2, a, c and V increase monotonically with the Mn concentration when $x < 0.05$. Further increasing the Mn concentration, the lattice parameters of $Zn_{1-x}Mn_xO$ do not change, which indicates that the solubility limit of Mn^{2+} in ZnO bulks is about 5%. The difference of the ionic radius between Mn^{2+} and Zn^{2+} may be the main reason that results in the lattice parameter's monotonic increase with the increase of the Mn concentration. On the other hand, the Mn^{2+} ion can easily change into Mn^{3+} to form the impurity phase of $ZnMn_2O_4$. Therefore an obvious impurity phase can be observed when the Mn concentration is larger than 5%. As described in Table 1, the Molar percent of impurity is 0.76% and 1.74% when the nominal Mn doping concentration is 7% and 10%, respectively.

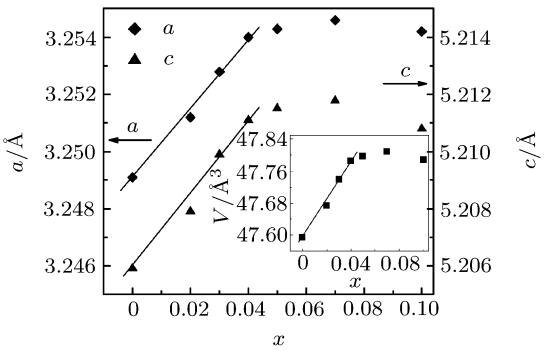


Fig.2. Mn content dependence of lattice parameters and unit cell volume (the inset) of $Zn_{1-x}Mn_xO$ bulks (1 Å=0.1 nm).

Table 1. Lattice parameters and the fitting results of $Zn_{1-x}Mn_xO$ bulks. The impurity phase is $ZnMn_2O_4$.

$Zn_{1-x}Mn_xO$ (x =)	0	0.02	0.03	0.04	0.05	0.07	0.10
O(1/3, 2/3, z)	0.38483	0.38432	0.38962	0.38658	0.38772	0.38532	0.38186
a/Å	3.24909	3.25120	3.25279	3.25400	3.25429	3.25459	3.25420
c/Å	5.20590	5.20790	5.20990	5.21110	5.21150	5.21179	5.21079
V/Å^3	47.59402	47.67416	47.73900	47.78550	47.79775	47.80924	47.78854
R_{wp}/%	7.002	7.654	7.812	7.701	7.421	13.801	11.417
χ^2/%	5.767	6.366	6.582	6.149	5.632	19.375	11.413
impurity phase/at%	0	0	0	0	0.23	0.76	1.74

Figure 3 shows a typical temperature dependence of magnetization for Zn treated $Zn_{0.97}Mn_{0.03}O$ bulk measured at an applied field of 1000 Oe (1 Oe=80 A/m). The solid line represents the Curie–Weiss law fit to the experimental data. As shown in the figure, the experimental data and the calculation show excellent agreement, which imply that the temperature dependence of magnetization obeys the Curie–Weiss law[13] $\chi = C/(T - \Theta)$, where C is the Curie constant and Θ is the Curie–Weiss temperature, respectively. The M–T curve obeying the Curie–Weiss law indicates that the samples are paramagnetic down to 5 K. The fitted result demonstrates that the Curie–Weiss temperature Θ for $Zn_{0.97}Mn_{0.03}O$ is –7.21 K, which implies that weak antiferromagnetic interaction exists in the samples. Meanwhile, the effective magnetic moment per Mn is about 0.505 (μ_B/Mn), which is smaller than the theoretical saturation magnetization for the Mn^{2+} spins assuming $S = 5/2$ and $g = 2$ (S is the spin quantum number and g is the Lande g factor). We consider the small magnetic moment per Mn is because of the weak antiferromagnetic interaction in the samples.

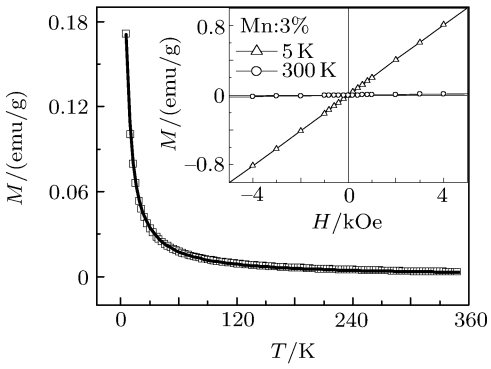


Fig.3. The temperature dependence of magnetization of $Zn_{0.97}Mn_{0.03}O$. The solid line represents the Curie–Weiss law fit to the data. The inset shows magnetization as a function of the applied field for the Zn treated $Zn_{0.97}Mn_{0.03}O$ at 5 K and 300 K, respectively.

The inset of Fig.3 displays the magnetization as a function of the applied field at 5 K and 300 K, respectively. No ferromagnetic behavior can be observed, which demonstrates again that the samples are paramagnetic. The as-prepared Mn doped ZnO bulks (without the Zn vapor treatment) have similar PM properties (not shown here), which is consistent with other previous reports.[8−12]

$Zn_{1-x}Mn_xO$ bulks were reported with room temperature ferromagnetism when they synthesized by a low temperature process,[16] but the origin of ferromagnetism might come from the impurity metastable phase.[17] Our $Zn_{1-x}Mn_xO$ bulk samples were synthesized by a high temperature process, and the XRD results show that all the samples are single phase when $x < 0.05$. This is to say that the single phase $Zn_{1-x}Mn_xO$ bulks are intrinsic PM, no matter whether the samples were treated by Zn vapor or not.

The samples without Zn vapor treatment are completely insulating. Therefore, the electrical transport behavior cannot be investigated. After Zn vapor treatment, the $Zn_{1-x}Mn_xO$ bulks display semiconductor behavior as shown in Fig.4. The resistance behavior is very complex, and it is impossible to fit the experimental data with a single conduction mechanism in the entire temperature range. Three conduction mechanisms were employed to describe the electrical transport behavior. As shown in Fig.4(b), the different Mn content samples exhibit the same resistance behavior. All the samples' resistance behavior was analyzed by the same process, and the sample $Zn_{0.96}Mn_{0.04}O$ was chosen as the representative to describe the fitted result as shown in Fig.4(a).

At low temperature, the resistivity increases extremely rapidly as temperature decreases. The temperature dependence of resistivity can be well fitted by the modified Mott's variable-range hopping (VRH) model[18]—the variable-range hopping (VRH)

of bound magnetic polarons (BMPs)[19]

$$\rho_1(T) = \rho_{01}\exp[(T_1/T)^{2/5}], \quad (1)$$

where $T_1 = [\beta/Ga^3]^{1/2}$, and β is a numerical factor of the order of unity, G is a joint density of (polaronic) states (DOS), a is the localization radius of the electron wave function. In this modified Mott's model, the well-known Mott's exponent 1/4 should be substituted with some larger exponent 2/5 for the bulk materials. The agreement between the experimental data and the calculation is excellent as seen in Fig.4(a). This result demonstrates that the variable-range hopping of the BMPs dominates the electrical transport behavior when the temperature is below 50 K.

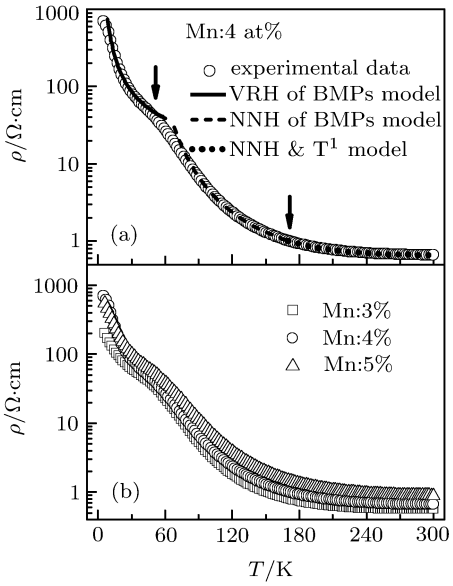


Fig.4. Typical temperature dependence of resistivity behavior for Zn treated $Zn_{1-x}Mn_xO$ (x = 0.03, 0.04 and 0.05).

When 90 K $< T <$ 170 K, the resistance behavior will obey nearest-neighbor hopping (NNH) of the magnetic polaron model,[20,21]

$$\rho(T) = \rho_{02}T\exp[(\varepsilon_2/kT)], \quad (2)$$

where ε_2 is the activation energy and k is the Boltzmann constant. The excellent agreement between the experimental data and the fitting results indicates that nearest-neighbor hopping (NNH) of BMPs dominates the electrical conduction when the temperature is below 170 K.

When $T >$ 170 K, the conduction mechanism becomes complicated, the resistivity data cannot be fitted by only one model. It needs an additional conduction term to best fit the data,

$$\rho(T) = \rho_{02}T\exp[(\varepsilon_2/kT)] + \rho_{03}\exp[(\varepsilon_3/kT)]. \quad (3)$$

The first term comes from the contribution of hopping of magnetic polarons. The second term shows the T^{-1} law, which would be characteristic of activation to a mobility edge in the semiconductors.[21,22]

The fitted result parameters for the resistance behavior are displayed in Table 2. From the table, we can see that all the samples' activation energy ε is very close to the ionization energy 0.05 (eV) of the Zn_i shallow donor.[23] This phenomenon proves that the carriers, which play a key role in the electrical transport behaviors, of our samples come from the Zn_i shallow donor. At the same time, the carriers trapped by any kind of attractive potential of a defect can form a 'cloud' of aligned spins of the surrounding magnetic atoms. The creation of such a complex was referred as BMPs.[19,24,25]

Table 2. The electrical transport fitted result.

	6–50 K		90–170 K		170–300 K			
Mn: at%	ρ_{01}/Ω·cm	T_1	ρ_{02}/Ω·cm	ε_2/eV	ρ_{02}/Ω·cm	ε_2/eV	ρ_{03}/Ω·cm	ε_3/eV
3	10.16	128.08	0.00026	0.042	0.00109	0.036	0.34614	0.021
4	3.230	583.64	0.00034	0.042	0.00099	0.041	0.27825	0.027
5	7.922	321.51	0.00047	0.044	0.00142	0.042	0.45859	0.026

From the electrical transport fitted result, it is clear that formation and transport of the BMPs are the key point to understanding the electrical transport behavior for the TM doped ZnO bulks. At high temperature, the electrical conduction is the combined result of nearest-neighbor hopping (NNH) of the BMPs and by activation above the mobility edge[22] which obeys the T^{-1} law. When $T <$ 170 K, the nearest-neighbor hopping of BMPs[19,24,25] among the impurity sites dominates the electrical conduction. When the temperature decreased below 50 K, the thermal energy is not great enough for the BMPs to hop to their nearest neighbor. In this case, it will be more favorable for the carriers (BMPs) to hop farther to

find a smaller potential difference. In this case, carrier hopping is always of variable-range type.[18,19]

Figure 5 shows the magnetic field dependence of the MR effect for different Mn concentrations at different temperatures. All the samples show positive MR effect and MR peaks at low temperature. At 5 K, the maximum MR value increases with the increase of Mn concentration within the solubility limit of Mn^{2+} in ZnO (about 5 at %) as seen in Fig.6. When temperature is above 50 K, the MR effect becomes weak rapidly.

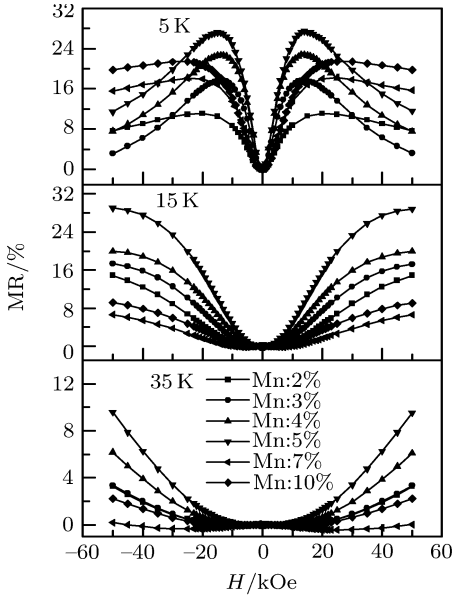


Fig.5. MR effect of Zn treated $Zn_{1-x}Mn_xO$ (x = 0.02, 0.03, 0.04, 0.05, 0.07, 0.10) bulks at various temperatures.

The large positive MR effect at low temperature is believed to come from the s–d exchange interaction induced spin-splitting.[25−28] The conduction band of the magnetic semiconductor will be split into two spin subbands under a magnetic field. In TM ion doped ZnO, the s–d exchange interaction induced spin-splitting will lead to a redistribution of the conduction carriers between the two subbands, which results in an increasing of the Thomas–Fermi screening radius. The increasing of Thomas–Fermi screening radius will lead to an increase in potential fluctuations and result in a higher degree of electron localization. The electron localization results in the increasing of the resistance. In this way, the samples show positive MR effect. At the same time, the positive MR effect increases with the increasing TM doping, indicating that the s–d exchange interaction will be enhanced with the increase of Mn concentration as shown in Fig.6.

On the other hand, the formation of BMPs is evident in the Mn doped ZnO bulks from the conduction mechanism analysis above. It is well known that the magnetic polarons in a pure magnetic polaron system grow in size and lead to the carriers' delocalization when a magnetic field is applied.[29] With the increase of the applied field, BMPs will be delocalized from the self-trapped state, which will induce an abrupt decrease of resistance. So the formation of the BMPs and the delocalization of BMPs will contribute to the negative MR effect. Meanwhile, the conductance increases if the spin-disorder scattering decreases due to enhanced alignment of spins of both magnetic ions and carriers.[28] Therefore, the suppression of spin-disorder scattering in a magnetic field might be another possible origin for the negative MR contribution in ZnO based DMSs.

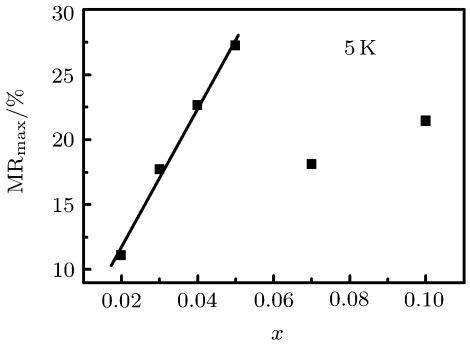


Fig.6. Maximum MR value (MR_{max}) at 5 K as a function of Mn concentration in Zn vapor treated samples.

At low magnetic field, the redistribution of the conducting carriers between the two subbands is sufficiently large to induce positive MR.[25−28] At high magnetic field, the conduction electrons' redistribution will become weaker when most of the conduction electrons are in the low-energy subband, and then the resistance turns to decrease with the increase of magnetic field due to the delocalization of BMPs and field suppressed spin-disorder scattering. In this way, a peak can be observed in the MR curve as shown in Fig.5.

As reported in our previous study on TM doped ZnO bulks,[13,30] the formation of BMPs is a universal phenomenon for ZnO based DMSs when the sample is in the localization range. The conduction mechanism and MR behavior of ferromagnetic $Zn_{1-x}Co_xO$ and paramagnetic $Zn_{1-x}Mn_xO$ bulks are very similar. This phenomenon reveals that BMPs alone are not enough to explain the magnetic property of TM doped ZnO DMSs. The impurity-band model[31] suggests that the TM doped ZnO samples exhibit ferromagnetism when a large density of 3d states is pinned in the donor impurity band at the Fermi level.[31]

In our previous paper, we further indicated that ferromagnetic TM doped ZnO DMSs should obey the Stoner criterion.[13] According to the Stoner criterion, the density of states near the Fermi level, $N(E_F)$, should be large enough to satisfy $N(E_F)I > 1$ (I stands for the Stoner parameter) for any ferromagnet. The Zn vapor treatment process will induce interstitial Zn, which is the donor impurity, into $Zn_{1-x}Co_xO$ bulk samples, and then further increase $N(E_F)$ near the Fermi level. As for $Zn_{1-x}Mn_xO$ bulk samples, it should have the same effect for Zn_i doping. However, the impurity band of Mn^{2+} is deeper than that of Co^{2+}.[32] This difference means that $N(E_F)$ near the Fermi level is finally not large enough to satisfy the Stoner criterion and then results in PM nature for $Zn_{1-x}Mn_xO$ bulk samples.

4. Summary

In summary, $Zn_{1-x}Mn_xO$ bulks were prepared by the solid state reaction method. The as-prepared samples were then subjected to the Zn treatment. XRD patterns show that the samples are single phase of wurtzite structure when the Mn concentration is below 5%. Unlike Zn treated Co doped ZnO bulks, the Zn vapor treatment cannot enable the Mn doped ZnO bulks to have ferromagnetism down to 5 K. But the samples change from completely insulating to semiconductor. The temperature dependence of resistance and the field dependence of magnetoresistance demonstrate that the BMPs play an important role in the electrical transport behavior. The hopping of BMPs dominates the electrical transport behavior when temperature is below 170 K. Large positive MR which increases with the increase of doping concentration has been observed, which indicates that the spin-splitting is enhanced by the substitution $3d$ ions. The positive MR effect is ascribed to the s–d exchange interaction induced spin-splitting, and the negative effect results from delocalization of BMPs and the magnetic field suppressed spin-disorder scattering.

References

[1] Pan F, Song C, Liu X J, Yang Y C and Zeng F 2008 *Mater. Sci. Eng.* R **62** 1 and references therein

[2] Dietl T, Ohno H, Matsukura F, Cibert J and Ferrand D 2003 *Science* **287** 1019

[3] Liu X C, Zhang H W, Zhang T, Chen B Y Chen Z Z, Song L X and Shi E W 2008 *Chin. Phys.* B **17** 1371

[4] Yu Z, Li X, Long X, Cheng X W, Wang J Y, Liu Y, Cao M S and Wang F C 2008 *Acta Phys. Sin.* **57** 4539 (in Chinese)

[5] Duan L B, Rao G H, Yu J, Wang Y C, Chu W G and Zhang L N 2007 *J. Appl. Phys.* **102** 103907

[6] Liu X C, Shi E W, Chen Z Z, Zhang H W, Zhang T and Song L X 2007 *Chin. Phys.* B **16** 1770

[7] Yang J J, Fang Q Q, Wang B M, Wang C P, Zhou J, Li Y, Liu Y M and Lü Q R 2007 *Acta Phys. Sin.* **56** 1116 (in Chinese)

[8] Kolesnik S and Dabrowski B 2004 *J. Appl. Phys.* **96** 5379

[9] Lawes G, Risbud A S, Ramirez A P and Seshadri R 2005 *Phys. Rev.* B **71** 045201

[10] Chen W, Zhao L F, Wang Y Q, Miao J H, Liu S, Xia Z C and Yuan S L 2005 *Solid State Commun.* **134** 827

[11] Rao C N R and Deepak F L 2005 *J. Mater. Chem.* **15** 573

[12] Yang J H, Zhao L Y, Zhang Y J, Wang Y X, Liu H L and Wei M B 2007 *Solid State Commun.* **143** 566

[13] Zhu T, Zhan W S, Wang W G and Xiao J Q 2006 *Appl. Phys. Lett* **89** 022508

[14] Schwartz D A and Gamelin D R 2004 *Adv. Mater.* **16** 2115

[15] Hunter B A 1998 *IUCC Powder Diffraction* **20** 21

[16] Sharma P, Gupta A, Rao K V, Owens F J, Sharma R, Ahuja R, Osorio Guillen J M, Johansson B and Gehring G A 2003 *Nature Matter* **2** 673

[17] Kundaliya D C, Ogale S B, Lofland S E, Dhar S, Metting C J, Shinde S R, Ma Z, Varughese B, Ramanujachary K V, Salamanca-Riba L and Vankatesan T 2004 *Nature Matter* **3** 709

[18] Shklovskii B I and Efros A L 1984 *Electronic Properties of Doped Semiconductors* (Berlin: Springer)

[19] Foygel M, Morris R D and Petukhov A G 2003 *Phys. Rev.* B **67** 134205

[20] Yang Z, Bao X, Tan S and Zhang Y 2004 *Phys. Rev.* B **69** 144407

[21] Mott N F and Davis E A 1979 *Electronic Processes in Non-crystalline Materials* (Oxford: Clarendon Press)

[22] Viret M, Ranno L and Coey J M D 1997 *Phys. Rev.* B **55** 8067

[23] Han J, Mantas P Q and Senos A M R 2002 *J. Eur. Ceram. Soc.* **22** 49

[24] Ohno H, Munekata H, Penney T, von Molnár S and Chang L L 1992 *Phys. Rev. Lett.* **68** 2664

[25] Wang J, Gu Z, Lu M, Wu D, Yuan C, Zhang S, Chen Y, Zhu S and Zhu Y 2006 *Appl. Phys. Lett.* **88** 252110

[26] Sawicki M, Dietl T, Kossut J, Igalson J, Wojtowicz T and Plesiewicz W 1986 *Phys. Rev. Lett.* **56** 508

[27] Jin Z, Fukumura T, Kawasaki M, Ando K, Saito H, Sekiguchi T, Yoo Y Z, Murakami M, Matsumoto Y, Hasegawa T and Koinuma H 2001 *Appl. Phys. Lett.* **78** 3824

[28] Jin Z, Hasegawa K, Fukumura T, Yoo Y Z, Hasegawa T, Koinuma H and Kawasaki M 2001 *Physica* E **10** 256

[29] Majumdar P and Littlewood P 1998 *Phys. Rev. Lett.* **81** 1314

[30] Peng X D, Zhu T and Wang F W 2009 *Acta Phys. Sin.* **58** 3274 (in Chinese)

[31] Coey J M D, Venkatesan M and Fitzgerald C B 2005 *Nature Matter* **4** 173

[32] Fichou D, Pouliquen J, Kossanyi J, Jakani M, Campet G and Claviere J 1985 *J. Electroanal. Chem.* **188** 167